Proceeding of the IEEE
International Conference on Robotics and Biomimetics
Dali, China, December 2019

A Magnetically Actuated Octopus-like Robot Capable of Moving in 3D Space

Yuguo Dai,[1] Dixiao Chen,[1] Shuzhang Liang,[1] Li Song,[1] Qi Qi[1] and Lin Feng[1,2,*]

***Abstract*—Magnetic driving is an excellent non-contact method that can penetrate through the human and the biological tissues without any damage. Also, micro-nano robots are expected to enter into the human body, which will bring about revolutionary development in robotics. Here we propose an octopus-like soft robot that is expected to be used in biomedical and engineering fields in the future. Firstly, we establish a magnetic control system, which uses the minimum number of coils. The system can respond quickly with high precision and can propel robot in 3D space utilizing the coupled field contributed by multiple electromagnets acting in concert. Based on the system, we designed an octopus-like robot with three legs. The robot can move freely without constraints in the workspace. We apply triangular wave gradient magnetic field, which makes the movement of the robot more stable and controllable. At the same time, the swing of the tail increases the moving precision of the robot and make the control easier.**

I. Introduction

Magnetic field can transmit without any media, therefore, it is promising for remote control in complicated environment [1-3]. Using magnetic control, non-contact manipulation can be realized and will considerably extend the operating scope compared with traditional methods. Since magnetic device can be miniaturized, this has high potential in medical area with limited damage [3]. This has attracted considerable attention in recent years, since it can be widely used in vivo microsurgery, biological monitoring, and drug delivery [4, 5].

The non-contact operation of micro-miniature robots has demonstrated great application prospects [6-10]. All these methods include the light fields propulsion [11], chemical energy, and acoustic radiation force driving [12], bioenergy propulsion. These methods have been used to manipulate a wide variety of small robots, for example the micro-assembly or object transportation [13], and demonstrate high precision in practical applications. Among these driving methods, the magnetic actuating technique is particularly promising, since the magnetic force can be controlled in three-dimensional(3D) space and can provide sufficient force.

Because the magnetic field **B** generated by different coils can be vector superimposed, magnetic field with any desired directions can be acquired [14]. Therefore, 3D distribution of the magnetic field can be achieved. Many magnetic systems have been built and have been used in a variety of applications. For example, the Helmholtz coil can generate uniform field, and magnetic field at different directions can be obtained, but the magnetic flux density is generally small. Maxwell coils can produce a uniform gradient magnetic field, and can control the robot using gradient force. However, these generated magnetic field usually possesses weak strength. In addition, permanent magnets are also used to control the small magnetic robot and show great applications[15]. For 3D control of microrobot, many magnetic control systems have been developed. Typical examples include the Octomag system that uses eight coils for retinal procedures [14] and the enhanced electromagnetic system with six coils for microparticles manipulation [16, 17]. These systems use several coils distribute in 3D space, and can generate magnetic field with any desired direction. We find that in many systems, the position of the coils coincides with the platonic polyhedra, for example the cube with the six coils and the eight coils with the regular octahedron, all these systems epitomize high degree of symmetry and order. However, if forces are used to control an unconstrained magnetic object, four magnetic sources are required for 3 degrees of freedom force control [18].

Since the magnetic field will react with any magnetic substance, a magnetic device can convert magnetic energies into kinetic movement and overcome viscous resistance. A variety of robots have been fabricated, and can change its posture, speed and direction by changing the frequency, size, direction of the magnetic field. Since robots of different structures will response entirely different in the magnetic field, this makes it possible to realize the multi-degree of freedom of a robot. For example, the mobile microgripper used to carry microgels [19], an untethered magnetic micro-robot that can move freely on a surface [20], the highly efficient magnetic nanoswimmer [21] and the small-scale soft robot with multimodal locomotion [22], all these robots demonstrate huge applications.

In this paper，inspired by the regular tetrahedron for its high degree of symmetry and order, we establish a magnetic control system using the minimum number of coils as shown in Fig. 1(a) and (b). The system is controlled by the computer using an PI control, which guarantees the field can respond in time. Since the iron core is soft magnetic materials, the hysteresis is negligible. Therefore, the direction and intensity of the magnetic field in the working area can be controlled precisely. Also, we fabricate an octopus-like robot that can

Research supported by the Natural Science Foundation of Beijing (Grant No.17L20128), and Beihang University, "Zhuobai" project, ZG216S1751 and ZG226S188D.

[1]School of Mechanical Engineering & Automation, Beihang University, Beijing, China

[2]Beijing Advanced Innovation Center for Biomedical Engineering, Beihang University, Beijing, China.

[*]Corresponding author E-mail address: (e-mail: linfeng@buaa.edu.cn).

978-1-7281-6321-5/19//$31.00 ©2019 IEEE

swim stably in 3D space. In order to offset the gravity, the structure is further improved with a bubble in the middle part of the robot as shown in Fig. 1(c). By using the established system, the robot will emerge desired time-varying postures under actuating magnetic fields and can swim in enclosed liquid environment. Since the gradient is the main driving force, the swing of the tail increases the stability of the robot when swimming in the working area.

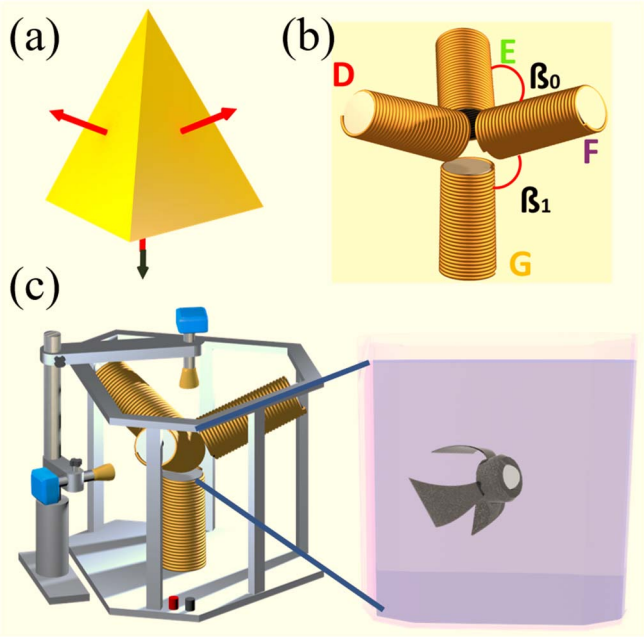

Fig. 1. (a) regular tetrahedron (c)distribution of the magnetic generating coils (c) diagram of the electromagnet system and the swimming octopus-like robot in the working area

II. Experiment Setup

A. System setup

Since the system is inspired by the regular tetrahedron, the angles of the four electromagnets are equal to each other as shown in Fig. 1: the angle $\beta 0$ between the upper three electromagnets and the angle $\beta 1$ between the upper electromagnets and the bottom electromagnets are both $arc\cos(-1/3)$, which reflects the highly symmetry of the system and this makes the control of the system easier.

The established magnetic control system is shown in Figure 2, and at the center of the four electromagnets is a spherical area with a diameter of 90 mm. Wherein the number of turns of the coils and the diameter of each electromagnet are the same, parameters for each of the electromagnets are provided in Table I. And the distance of each electromagnet to the origin of the working area are the same, and the end faces of each electromagnet are tangent to a spherical region. Two CCD cameras (HT2000CN) are placed on the side and the top respectively, which can observe the 3D posture of the robot from different views in real time and transfer the video to the computer. In addition, the system also includes a computer control section, an AD/DA conversion module (using a data acquisition system: USB-6211, National Instruments Inc.), a circuit amplification section (motor driver DZRALTE-040L080) achieving real-time control of the magnetic field.

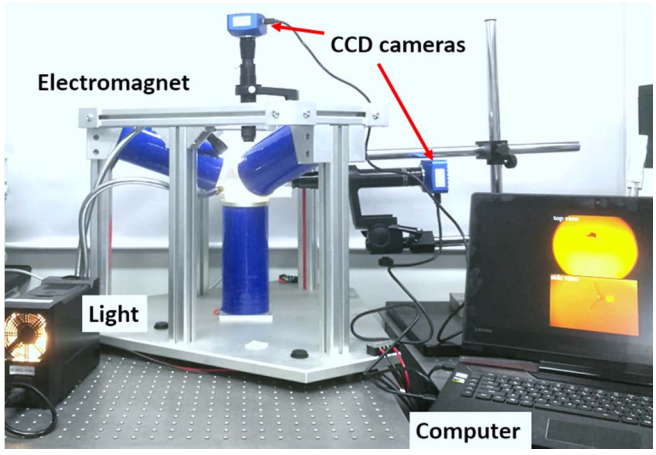

Fig. 2. Diagram of the electromagnet system, including the magnetic field generation part, the computer controlling part, and the image acquisition part.

III. Electromagnet Properties

Description	Value	Units
Number of Turns	914	---
Distance from Center	0.045	*m*
Diameter of Wire	2.24	*mm*
Coil Resistance	1.0	Ω
Core Inner Diameter	0.055	*m*
Core Outer Diameter	0.090	*m*
Coil Length	0.220	*m*
Maximum Current	15	*A*
Diameter of Working Area	90	*mm*

B. Magnetic control

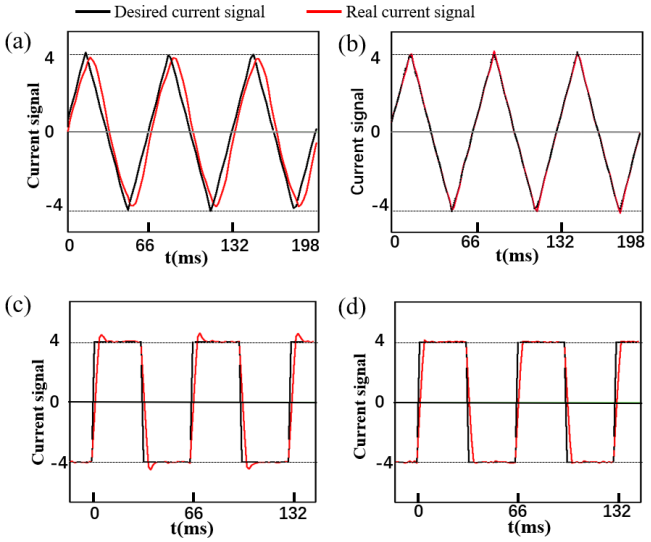

Fig.3 PI control (a) and (c) shows the desired current signal and the output signal (measured) before K_P and K_I are adjusted (15 Hz). (b) and (d) shows the signal after the K_P and K_I are adjusted

Since the magnetic flux density B is controlled by the magnitude of the current, it is necessary to make the output current coincide with the expected current. In this system, the

inductive reactance will increase due to the iron core, which makes the control more complicated. To make the output current consistent with the desired signal, we use PI control. By adjusting the values of K_P and K_I, where K_P can guarantee the correspondence between the output signal and the input signal and K_I can eliminate the deviation, the output current can follow the input signal in time. We input triangle wave and square wave signal separately (15Hz, with the amplitude of 4A) and it can be found that there is a large error between input and output before adjustment, as shown in Figure 3(a) and (c). After adjusting K_P and K_I, the output signal can respond well to the input signal as shown in Figure 3(b) and (d).

In fact, for a constant current element in space, the magnetic field generated is only related to the magnitude of the current in the coil. The magnetic flux density can be expressed as:

$$dB = \frac{\mu_0}{4\pi} \cdot \frac{Idl \times e_r}{r^2} \quad (1)$$

Where Idl represents a current source of constant current, r represents a radial vector pointing from a current element to the point P, $\mu_0 = 4\pi \times 10^{-7} N/A^2$, indicating the magnetic permeability of free space. When the current source is loop-integrated, the magnetic field of a loop coil on its axis can be obtained:

$$B = \left(\frac{\mu_0 R^2}{2(R^2+x^2)^{3/2}}\right) * I \quad (2)$$

Where R is the radius of the coil and x is the distance from a point on the axis to the center of the coil.

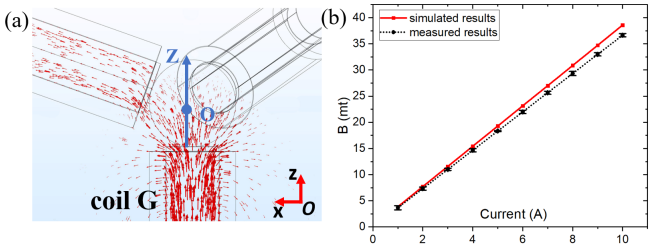

Fig. 4. (a) distribution of magnetic induction line (b) experimental and simulation results of the magnitude of B at Z= 0 mm, when only electromagnet G is energized.

The presence of the core greatly enhances the strength of the magnetic field, causing the magnetic field to be stronger several or even tens times. Since the iron core generally has a hysteresis effect, the magnetic field does not always have a linear relationship with the magnitude of the current, which makes the control complicated. But for soft magnetic materials, the situation is different. For some soft magnetic materials like iron, the hysteresis is negligible within a certain range. In the newly established system, when an electromagnet is energized, the magnetic field generated by it will magnetize the core of the remaining electromagnets, so that the size and distribution of the magnetic field will change. As shown in Fig. 4(a), when only coil G is energized, the distribution of the magnetic induction line will change due to the presence of the iron core, which can increase the strength of the magnetic field in the working area.

Fig. 4(b) illustrates the experimentally measured data and the simulation results of the magnetic flux density at the central point. It can be seen that the magnetic field generated by the electromagnet is proportional to the magnitude of the current. In fact, there is almost no hysteresis effect, and the linearity is very good. The deviation between the experimental and the simulation results might be caused by factor such the model uncertainty and the environment. In the system, the magnetic flux density $B_P = [B_x \quad B_y \quad B_z]^T$ at any point P in the working area can be expressed as the vector sum of the magnetic fields generated by all the coils:

$$\boldsymbol{B}_P = \sum_e^{D,E,F,G} \boldsymbol{B}_e i_e \quad (3)$$

Where e is the code number of an electromagnet in the system, which can be taken as D, E, F, and G, i_e is the current flowing through the coil e, and B_e is the magnetic flux density generated by the unit current of a electromagnet in the system.

IV. Robot Model

A. Robot Fabrication

Based on the magnetic system, we designed the octopus-like robot that can achieve three-dimensional motion. Firstly, we obtain the mold using 3D printing technology (photosensitive resin material). There is a cavity structure in the head of the robot to increase the buoyant force in the liquid environment, as shown in Fig. 5(a). The liquid will not enter the cavity even if the cavity is not closed since the size of the cavity is very small. As a kind of magnetic material, NdFeB powder with diameters of 5.0 μm (density ρ=7.61 g/cm3, Magnequench), has excellent magnetic properties, with a remanence Br of 838–878 mT. Firstly, the NdFeB powder is mixed into ecoflex00-10 (A and B glues were mixed together in a 1:1 ratio) with a mass fraction of 15% to obtain the liquid magnetic material. Subsequently, the liquid is poured into the model, as shown in Fig. 5(b), which will solidify after approximately 2 h at 30 ℃. After solidification, take the robot out and the octopus-like robot will be obtained as shown in Fig. 5(c). For the purpose of having a robot with the required magnetization curve, the robot is then placed in a transparent tube with a diameter of 1.6 mm, since the diameter of head of the robot is around 1.5mm. The tail of the robot will deform, then put the tube in a strong magnetic field (the magnetic flux density reaches 1.6T), as shown in Fig. 5(d) and (e).

Since the NdFeB material has a high residual magnetization, when the strong magnetic field diasppeared, the robot itself will maintain the magnetization profile and will not be re-magnetized in the weak magnetic field. After the robot is taken out of the tube, the robot tail will return to its original shape due to the elastic modulus, and the magnetization profile is shown in Fig. 5(f). Thereby a robot with the required magnetized profile is obtained. When an external magnetic field is applied, the magnetization direction in the tail of the robot will keep in alignment with the magnetic field, which makes the tail of the robot bend.

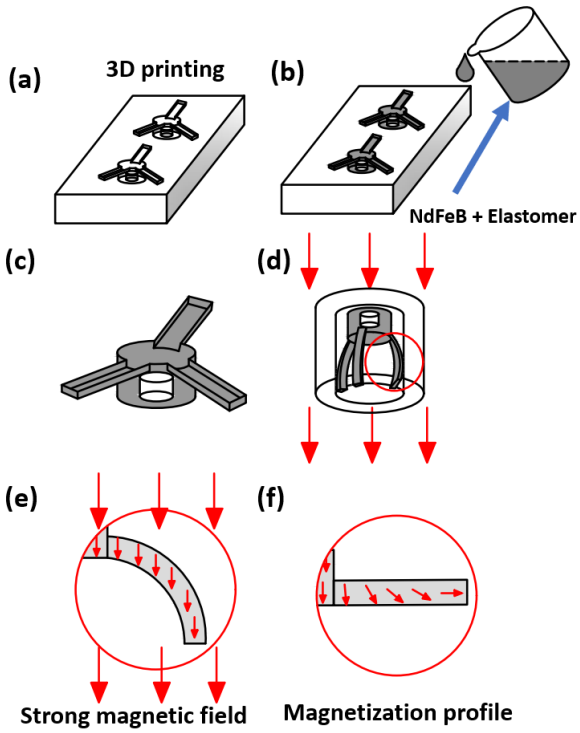

Fig. 5 (a)-(c)Schematic diagram of the manufacturing process of the octopus-like robot; (d)-(e) the magnetization process; (f) the magnetization profile of the octopus-like robot.

B. *Robot Analysis*

In fact, any magnetic substance in the magnetic field will be subjected to the magnetic force F and the magnetic moment T, wherein the magnetic force will lead to the movement of the magnetic substance, and the magnetic moment will cause the rotation of the magnetic substance. The magnetic force is proportional to the magnetic field gradient, while the magnetic moment is proportional to the magnetic flux density B. For a magnetic element, the magnetic force f and magnetic moment τ can be calculated by the following formula:

$$\boldsymbol{\tau} = \boldsymbol{m} \times \boldsymbol{B} \tag{4}$$

$$\boldsymbol{f} = (\boldsymbol{m} \cdot \nabla)\boldsymbol{B} \tag{5}$$

Where m represents the magnetization of the element, $\nabla = \left[\frac{\partial}{\partial x} \quad \frac{\partial}{\partial y} \quad \frac{\partial}{\partial z}\right]^T$, $B = [B_x \quad B_y \quad B_z]^T$

Since there is no current in the working space, the force of the micro-element in the magnetic field is available from Maxwell's equation[18]:

$$\boldsymbol{f} = (\boldsymbol{m} \cdot \nabla)\boldsymbol{B} = \begin{bmatrix} \frac{\partial B_x}{\partial x} & \frac{\partial B_x}{\partial y} & \frac{\partial B_x}{\partial z} \\ \frac{\partial B_x}{\partial y} & \frac{\partial B_y}{\partial y} & \frac{\partial B_y}{\partial z} \\ \frac{\partial B_x}{\partial z} & \frac{\partial B_y}{\partial z} & -(\frac{\partial B_x}{\partial x} + \frac{\partial B_y}{\partial y}) \end{bmatrix} \boldsymbol{m} \tag{6}$$

$$\boldsymbol{\tau} = \boldsymbol{m} \times \boldsymbol{B} = \begin{bmatrix} 0 & B_z & -B_y \\ -B_z & 0 & B_z \\ B_y & B_x & 0 \end{bmatrix} \boldsymbol{m} \tag{7}$$

The force of the magnetic elements in the magnetic field can be obtained by the above formula. Since the magnetization m of the element can be expressed as:

$$\boldsymbol{m} = \frac{d\boldsymbol{M}}{dV} \tag{8}$$

where M present the magnetization magnitude of the robot. Therefore, the total magnetic force F and magnetic moment T can be expressed as:

$$\boldsymbol{T} = \int \boldsymbol{\tau} dV \tag{9}$$

$$\boldsymbol{F} = \int \boldsymbol{f} dV \tag{10}$$

For the octopus-like robot, for better observation, the robot is put in a transparent resin environment. Since the head of the robot is designed with a cavity structure, in return a bubble will produce within the cavity structure, so that the gravity could be offset by the buoyant force, as shown in Fig. 6, where gravity $G = F_{float}$. When the robot is placed in a gradient magnetic field, the robot will move forward in the gradient direction. And the robot will always accelerate until the magnetic force $\boldsymbol{F}$ is balanced with the resistance, which increases the complexity of the control. Therefore, we choose the triangular waveform to drive the robot, which will increase the moving accuracy and make it easier to control.

Also, since the robot is made of NdFeB material, it will remain the magnetization profile after being magnetized. When there is no magnetic field, the tail of the robot will remain in its original state; if the magnetic field is applied, the tail will be bend due to the magnetic moment $\boldsymbol{T}$. Due to the symmetry of the three tails, the overall magnetic moment of the robot is zero.

By applying the triangle magnetic field, the tail of the robot will periodically change seems like it's swimming. When the field is on, the gradient force will propel the robot to move and the tail of the robot will bend which will decrease the resistance of the liquid environment. However, when the field is off, which means we want to stop the movement of the robot, the tail of the robot will stretch that increases the resistance, making the robot's motion control more sensitive. Also, the tail's swing causes a reverse flow of liquid, which pushes the robot forward. The movement of the robot is a totally result of the gradient field and the oscillation of the tail, where the gradient field accounts for the main contribution.

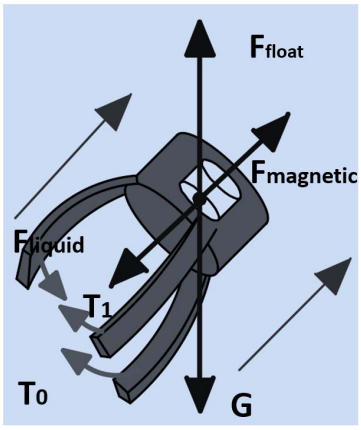

Fig. 6 Schematic diagram of the force of the 3D octopus-like robot when the magnetic field B is applied.

V. Experiment and Results

A. Bending of the tail

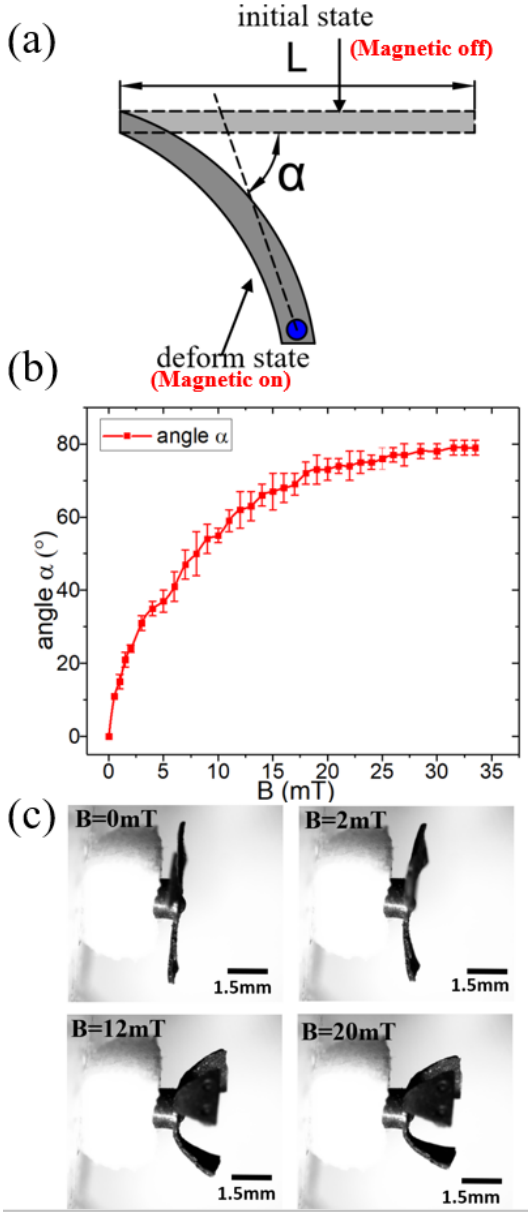

Fig. 7 (a) the tail's different posture when there is magnetic field is on and off (b) the relationship between the angle α and the magnetic field. (c) the image of the robot at different magnetic field

Since the octopus-like robot is magnetized in a strong magnetic field, it will remain the magnetization curve when the strong magnetic field disappeared. Therefore, when there is no magnetic field, the robot will remain its initial state. When an external magnetic field is applied, the tail of the robot will be deformed to align with the external magnetic field as shown in Fig. 7(a), which illustrates the initial state and the deform state of the robot tail, where α is the bending angle of the end of the robot's tail. If the external magnetic field is periodic, like a triangle wave, the tail of the robot will periodically change seems like it's swimming. Fig. 7(b) shows the relationship between the angle α and the magnetic field. It can be seen that when the magnetic field increase, as a result the angle will become larger, at first it changes quickly, but when the angle is around 80°, it will increase slightly or even not change. This is because the angle between the magnetic field and the magnetization direction of the tail decreases, the magnetic moment becomes smaller, and a much larger magnetic field is required to increase the bending angle. Fig. 7(c) shows the state of the robot when in magnetic field of different flux intensity.

B. 3D movement of the robot

After placing the robot in the working area of the magnetic system, since the robot itself has been magnetized, it will move forward under the gradient magnetic field, and its tail will also bend due to the external magnetic field. When the periodically oscillating magnetic field is applied, the tail of the robot will periodically bend, which will also provide a forward force. Fig. 8 illustrates the robot moving in the liquid environment, where (a) and (b) are the top view of the robot while (c) and (d) is the side view (see video 1). By controlling the magnetic field generated by these electromagnets, the robot can be moved in different directions.

The asymmetrical tail motion of the robot increases the motion posture of the robot while providing auxiliary power. However, as the magnetic field at the working area is a gradient rather than a uniform field, the main driving force is the gradient force. By applying an oscillating magnetic field，the robot can move more stable, guaranteeing the robot with higher position precision. When the robot is moving forward and the field is on, the bending of its tail will reduce resistance while the swing provides additional propulsion. When the field is off, the tail of the robot will unfold, which will undoubtedly increase the resistance of the liquid, which helps stops the robot making the robot moving more stably.

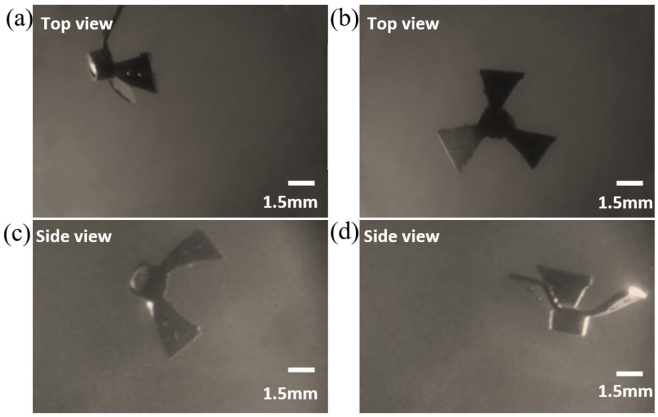

Fig. 8 The movement of the robot in the closed transparent resin environment. By adjusting the magnetic field, the robot can reach any position in the space. Figures (a)(b) show the top view of the robot and (c)(d) is the side view.(see video 1)

VI. Conclusion And Discussions

In this paper, we show a magnetic control system for noncontact control of octopus-like robot. This developed system uses the minimum number of coils which take the structure of a regular tetrahedron, and can respond quickly for real-time control with high accuracy. Also, the system has high

precision of control when propelling magnetic object in 3D space.

At the same time, we make an octopus-like robot which can achieve three-dimensional motion. The octopus-like robot is designed particularly that its gravity could be balanced by its buoyancy. The 3D movement of the robot can be realized by the gradient field and the swing of its own tail. The robot's tail will bend that increases the moving precision and provide forward force.

Future work includes optimizing the control of magnetic fields and exploring the moving speed of the robot in different environments and track the robot in real-time.

REFERENCES

[1] H. W. Tung, M. Maffioli, D. R. Frutiger, K. M. Sivaraman, S. Pane, and B. J. Nelson, "Polymer-Based Wireless Resonant Magnetic Microrobots," *Ieee Transactions on Robotics,* vol. 30, no. 1, pp. 26-32, Feb, 2014.

[2] S. Martel, "Beyond imaging: Macro- and microscale medical robots actuated by clinical MRI scanners," *Science Robotics,* vol. 2, no. 3, Feb 15, 2017.

[3] M. Sitti, "MINIATURE DEVICES Voyage of the microrobots," *Nature,* vol. 458, no. 7242, pp. 1121-1122, Apr 30, 2009.

[4] L. Feng, S. Z. Liang, X. C. Zhou, J. L. Yang, Y. G. Jiang, D. Y. Zhang, and F. Arai, "On-chip microfluid induced by oscillation of microrobot for noncontact cell transportation," *Applied Physics Letters,* vol. 111, no. 20, Nov 13, 2017.

[5] L. Feng, S. Y. Zhang, Y. G. Jiang, D. Y. Zhang, and F. Arai, "Microrobot with passive diamagnetic levitation for microparticle manipulations," *Journal of Applied Physics,* vol. 122, no. 24, Dec 28, 2017.

[6] S. Tasoglu, E. Diller, S. Guven, M. Sitti, and U. Demirci, "Untethered micro-robotic coding of three-dimensional material composition," *Nature Communications,* vol. 5, Jan, 2014.

[7] G. Z. Lum, Z. Ye, X. G. Dong, H. Marvi, O. Erin, W. Q. Hu, and M. Sitti, "Shape-programmable magnetic soft matter," *Proceedings of the National Academy of Sciences of the United States of America,* vol. 113, no. 41, pp. E6007-E6015, Oct 11, 2016.

[8] H. W. Huang, M. S. Sakar, A. J. Petruska, S. Pane, and B. J. Nelson, "Soft micromachines with programmable motility and morphology," *Nature Communications,* vol. 7, Jul, 2016.

[9] L. Feng, Y. L. Sun, C. Ohsumi, and F. Arai, "Accurate dispensing system for single oocytes using air ejection," *Biomicrofluidics,* vol. 7, no. 5, Sep, 2013.

[10] Y. Y. Chen, Y. Z. Feng, J. D. Wan, and H. S. Chen, "Enhanced separation of aged RBCs by designing channel cross section," *Biomicrofluidics,* vol. 12, no. 2, Mar, 2018.

[11] M. H. Shabestari, A. E. C. Meijering, W. H. Roos, G. J. L. Wuite, and E. J. G. Peterman, "Recent Advances in Biological Single-Molecule Applications of Optical Tweezers and Fluorescence Microscopy," *Single-Molecule Enzymology: Nanomechanical Manipulation and Hybrid Methods,* vol. 582, pp. 85-119, 2017.

[12] D. Ahmed, C. Dillinger, A. Hong, and B. J. Nelson, "Artificial Acousto-Magnetic Soft Microswimmers," *Advanced Materials Technologies,* vol. 2, no. 7, Jul, 2017.

[13] J. Rahmer, C. Stehning, and B. Gleich, "Spatially selective remote magnetic actuation of identical helical micromachines," *Science Robotics,* vol. 2, no. 3, Feb 15, 2017.

[14] M. P. Kummer, J. J. Abbott, B. E. Kratochvil, R. Borer, A. Sengul, and B. J. Nelson, "OctoMag: An Electromagnetic System for 5-DOF Wireless Micromanipulation," *Ieee Transactions on Robotics,* vol. 26, no. 6, pp. 1006-1017, Dec, 2010.

[15] L. Feng, P. Di, and F. Arai, "High-precision motion of magnetic microrobot with ultrasonic levitation for 3-D rotation of single oocyte," *International Journal of Robotics Research,* vol. 35, no. 12, pp. 1445-1458, Oct, 2016.

[16] J. Y. Li, X. J. Li, T. Luo, R. Wang, C. C. Liu, S. X. Chen, D. F. Li, J. B. Yue, S. H. Cheng, and D. Sun, "Development of a magnetic microrobot for carrying and delivering targeted cells," *Science Robotics,* vol. 3, no. 19, Jun 27, 2018.

[17] F. Z. Niu, J. Y. Li, W. C. Ma, J. Yang, and D. Sun, "Development of an Enhanced Electromagnetic Actuation System With Enlarged Workspace," *Ieee-Asme Transactions on Mechatronics,* vol. 22, no. 5, pp. 2265-2276, Oct, 2017.

[18] A. J. Petruska, and B. J. Nelson, "Minimum Bounds on the Number of Electromagnets Required for Remote Magnetic Manipulation," *Ieee Transactions on Robotics,* vol. 31, no. 3, pp. 714-722, Jun, 2015.

[19] S. E. Chung, X. G. Dong, and M. Sitti, "Three-dimensional heterogeneous assembly of coded microgels using an untethered mobile microgripper," *Lab on a Chip,* vol. 15, no. 7, pp. 1667-1676, 2015.

[20] C. Pawashe, S. Floyd, and M. Sitti, "Modeling and Experimental Characterization of an Untethered Magnetic Micro-Robot %J Int. J. Rob. Res," *International Journal of Robotics Research,* vol. 28, no. 8, pp. 1077-1094, 2009.

[21] T. L. Li, J. X. Li, K. I. Morozov, Z. G. Wu, T. L. Xu, I. Rozen, A. M. Leshansky, L. Q. Li, and J. Wang, "Highly Efficient Freestyle Magnetic Nanoswimmer," *Nano Letters,* vol. 17, no. 8, pp. 5092-5098, Aug, 2017.

[22] W. Q. Hu, G. Z. Lum, M. Mastrangeli, and M. Sitti, "Small-scale soft-bodied robot with multimodal locomotion," *Nature,* vol. 554, no. 7690, pp. 81-85, Feb 1, 2018.